The role of ion-water interactions in determining the Soret coefficient of LiCl aqueous solutions

Silvia Di Lecce[a], Tim Albrecht,[a] and Fernando Bresme[a,b,*]

The application of a thermal gradient to an aqueous electrolyte solution induces the Soret effect, and the salt migrates towards hot (thermophilic) or cold regions (thermophobic). Experimental studies of LiCl reported changes in the sign of the Soret coefficient as well as a minimum in this coefficient at specific salt concentrations and temperatures. At the minimum the thermodiffusive response of the solution is enhanced significantly. We have performed non-equilibrium molecular dynamics simulations of LiCl solutions to quantify the dependence of the sign change and minimum of the Soret coefficient with salt concentration and temperature. We find that the ion mass plays a secondary role in determining the magnitude of the Soret coefficient, while the diameter of the cation has a significant impact on the coefficient and on the observation of the minimum. Our simulations show that the ordering of water around Li^+ plays a key role in determining the Soret coefficient of LiCl salts.

Introduction

Temperature gradients give rise to fascinating coupling effects.[1] In pure molecular fluids, the heat flux can induce a preferred orientation in the molecules, the thermal orientation effect. In water the orientation results in electrostatic fields or thermal polarization, which can be particularly strong near a critical point.[2–5] In fluid mixtures and suspensions, thermal gradients drive thermodiffusion and thermophoresis, respectively, the so-called Ludwig-Soret (LS) effect[6,7]. The thermal gradient induces the motion of the solute towards hot or cold regions, depending on the average temperature of the fluid. Although the thermophoretic response is small as compared with that obtained with electrostatic fields, *e.g.* electrophoresis, it is in comparison much more sensitive to the nature of solute-water interactions. This feature has been exploited in the design of thermophoretic analytical devices.[8,9]

The strength of the thermodiffusion response can be quantified via the Soret coefficient $s_T = D_T/D$, which is defined by the ratio between the thermal diffusion, D_T, and the diffusion, D, coefficients. Experimental studies indicate that the Soret coefficient of aqueous solutions is of the order of 10^{-3} K^{-1} [10–13] and that the coefficient changes sing at a specific temperature, T_0, at which $s_T = 0$[14,15]. This "inversion temperature", T_0, defines a region where the thermophoretic response of the solution changes significantly. In alkali halide solutions when $s_T < 0$ for $T < T_0$ the solution becomes thermophilic (the solute migrates towards the hot region), while at $T > T_0$ the solution becomes thermophobic, $s_T > 0$, and the solute migrates towards cold regions. Sign changes of the Soret coefficient have been observed in a variety of systems: alkali halide solutions,[12] mixtures of organic liquids, such as benzene–cyclohexane[15] and aqueous protein solutions[16] and ternary mixtures of poly(ethylene oxide), ethanol and water.[14]

Non-equilibrium thermodynamics[1,17,18] provides a general theoretical framework to rationalize thermal coupling effects such as the LS effect. Still, there is significant scope to expand our theoretical understanding of these phenomena, by linking the experimental behaviour, *e.g* in aqueous solutions, to specific solute-solvent interactions. In this context, microscopic approaches, such as molecular simulations, can be of particular help since it is possible to analyse the dependence of the thermophoretic response with systematic changes of the solute-water interactions.

In this article, we investigate the Soret coefficient of alkali halide solutions. There is a good number of experiments that offer a consistent view of the general dependence of the Soret coefficient with temperature. Early works using thermogravitational columns[10,19] indicated that the Soret coefficient of alkali halide solutions features the temperature inversion effect. More recently, sophisticated convection-free methods, such as Thermal Diffusion Forced Rayleigh Scattering (TDFRS),[14,20] have allowed further investigation of the thermodiffusion behaviour of alkali halide solutions. TDRFS and molecular dynamics simulations have confirmed the existence of a temperature inversion in alkali halide aqueous solutions.[12]. Temperature inversion effects have also been observed in aqueous suspensions, DNA molecules,[21]

[a] *Department of Chemistry, Imperial College London, London, SW7 2AZ, United Kingdom.*
[b] *Department of Chemistry, Norwegian University of Science and Technology, Trondheim, Norway.*
e-mail: silvia.di-lecce12@imperial.ac.uk, f.bresme@imperial.ac.uk

proteins,[16] and polymers,[22] using TDRFS or other experimental approaches. Brenner[23] attempted to rationalize the observed thermodiffusion response in terms of the thermal expansion of water. This is an interesting idea as it allows to establish a correlation between the temperature inversion effect and the temperature of maximum density of water, at which the thermal expansion changes sign. However, experiments of colloidal suspensions[24] and computer simulations of aqueous solutions[12] have not confirmed such correlation. This fact highlights our limited theoretical understanding of thermophoretic phenomena.

The early experiments performed with thermogravitational columns reported minima in the Soret coefficient of NaCl and KCl solutions.[10] These minima appeared at concentrations $< 10^{-1}$ mol kg^{-1} for NaCl, and between 0.1 and 1 mol kg^{-1} for KCl. More recently, a sharp minimum in the Soret coefficient of LiCl solutions was reported at salt concentrations close to 1 mol kg^{-1}.[11] The minimum has been corroborated using non-equilibrium molecular dynamics simulations.[25] In all these studies, the minimum appears in the thermophilic regime, $s_T < 0$. Water-ion interactions are expected to play a key role in defining the thermodiffusive response of the solution, and the observation of a minimum in the Soret coefficient. Therefore, we focus in this work on the investigation on LiCl-water interactions and their impact on the thermophoretic response of the solution. The solvation structure of LiCl solutions is of significant interest, as indicated by recent neutron scattering studies.[26]

We have employed Non-Equilibrium Molecular Dynamics (NEMD) simulations for our study. NEMD has advanced significantly in the last years. It is now possible to quantify the Soret coefficients of alkali halide aqueous solutions reproducing their experimental behaviour.[12,25] We have taken advantage of these computational developments to quantify the Soret coefficient of LiCl and to establish correlations between the coefficient and the mass and size of the ions.

Our article is organized as follows. We discuss in Section 2 the NEMD simulation approach to investigate aqueous solutions under thermal gradients. In Section 3 we present our results for the Soret coefficient and solvation structure of LiCl salt solutions. An analysis of the dependence of the minimum with the ion properties, size, and mass, follows. A final section with our conclusions and final remarks closes the paper.

Methodology

Non-Equilibrium Molecular Dynamics simulations were implemented following the method reported in ref. 27. We define three regions (see Fig. 1), with two thermostatting volumes. The temperature of the molecules inside the thermostats is adjusted to predefined hot and cold values by direct thermostatting, in order to set up a stationary temperature gradient.

We used two implementations of the NEMD approach. In the RESTRAINED (RES) case, we restrained (using a harmonic potential with force constant of 1000 kJ mol^{-1} nm^{-2}) the position of the oxygen atoms in the water molecules in the hot and cold thermostatting regions. The restrain applies only in the direction of the heat flux, z, while the molecules are free to move in the perpendicular directions, x and y. The restrained water molecules can rotate freely. To impose the thermal gradient we apply every timestep the v-rescale algorithm.[28] The RES simulations were performed with a modified version of GROMACS v. 4.6.3.[29] Additional simulations were performed following the approach discussed in ref. 30, using the LAMMPS code[31]. These simulations do not involve restraining. Instead, the atomic velocities are rescaled whenever a molecule enters any of the thermostatting regions. The molecules are free to move in and out of these regions. We will refer to these simulations as UNRESTRAINED (UNRES). In this instance, the thermal gradient was generated by using local thermostats too. The thermostats were applied every time step to the molecules inside the "hot" or "cold" thermostatting regions, using a simple velocity rescaling method. The linear momentum of the simulation box was reset every time step after each rescaling event. We find that the NEMD results

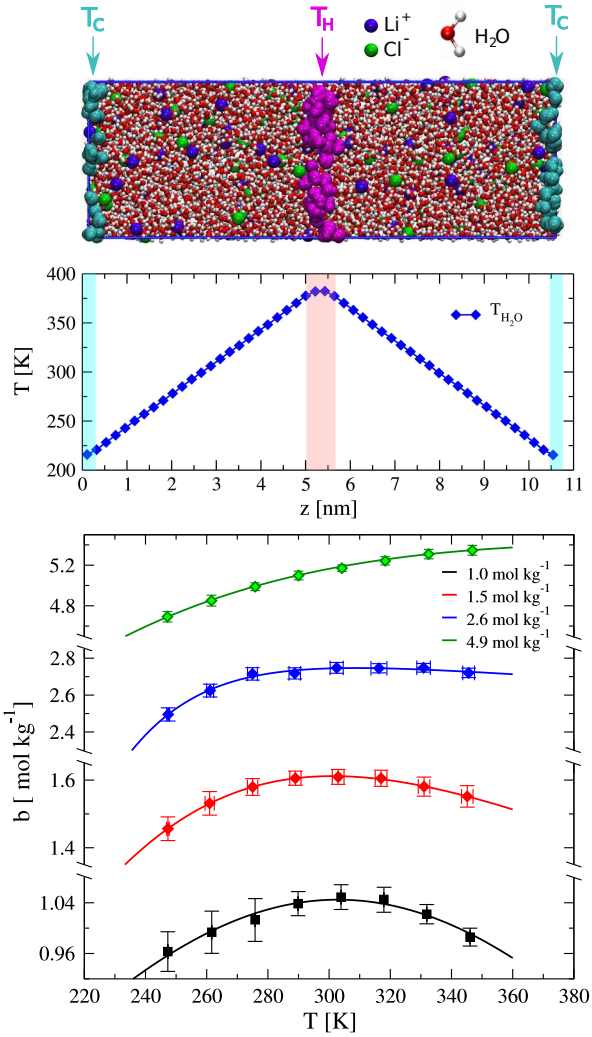

Fig. 1 (top) Snapshot of a LiCl solution under a thermal gradient showing the ions, (green – Cl^-, violet – Li^+) and water (white – hydrogen, red – oxygen). The thermostatting layers (see Methodology section and RES method) are highlighted in cyan (cold layer) and magenta (hot layer). The Middle and Bottom panels show the temperature of the unrestrained water molecules and the molality profiles at the stationary state at 600 bar and for several salt concentration (see legend).

are independent of the type of thermostat, v-rescale or a simple rescaling algorithm, used. To simulate the aqueous solutions we follow the method in ref. 25. All the simulations were performed in a prismatic box with lengths, $\{L_x, L_y, L_z\}/L_x = \{1,1,3\}$, and $L_x = 3.55$ nm (see Fig. 1). The system size varied between 4306 and 4484 water molecules and 77 to 385 ion pairs, in order to generate LiCl solutions with average concentrations in the range 1.0 – 5.6 mol kg^{-1}.

The ion-ion and ion-water interactions were described using the Coulombic and Lennard-Jones potentials,

$$U_{\alpha\beta}(r) = 4\varepsilon_{\alpha\beta}\left[\left(\frac{\sigma_{\alpha\beta}}{r}\right)^{12} - \left(\frac{\sigma_{\alpha\beta}}{r}\right)^{6}\right] + \frac{q_\alpha q_\beta e^2}{4\pi\varepsilon_0 r} \qquad (1)$$

where $U_{\alpha\beta}$ is the potential energy between atoms of species α and β, separated by a distance r, ε_0 is the vacuum permittivity and e is the electron charge. Standard combining rules were used to compute the cross interactions between different species: $\sigma_{\alpha\beta} = (\sigma_{\alpha\alpha} + \sigma_{\beta\beta})/2$, $\varepsilon_{\alpha\beta} = \sqrt{\varepsilon_{\alpha\alpha}\varepsilon_{\beta\beta}}$, where $\sigma_{\alpha\alpha}$ and $\varepsilon_{\alpha\alpha}$ represent the effective diameter and interactions of atoms of type α.

To model the water and LiCl interactions we employed the SPC/E model[32] and the force field by Dang *et al.*,[33–36] respectively. These models have been tested extensively in simulation studies of aqueous interfaces.[37] They predict water coordination numbers for Li^+ compatible with a tetrahedral arrangement of water molecules. This coordination number agrees with results obtained from accurate density functional theory computations.[38]

The Lennard-Jones interactions were truncated at $r_c = 1.5$ nm, and the Coulombic forces were computed in the RES case using the particle-mesh Ewald method (PME),[39] with a mesh width of 0.12 nm and an interpolation order of 4. For the UNRES case, we employed the Particle-Particle-Particle-Mesh (PPPM) method.[40] The equations of motion were integrated using the Leap-Frog and Velocity-Verlet algorithms in the RES and UNRES cases, respectively. We used in both cases an integration time step of 2 fs.

The simulation was set up as follows. First, a box of water was pre-equilibrated for 1 ns in the NPT ensemble, at 600 bar or 100 bar, and temperature, $T = (T_{COLD} + T_{HOT})/2$, where T_{COLD} and T_{HOT} are the temperatures in the NEMD simulations. Then we added ions to achieve the desired concentration, and we equilibrated again the whole system in the NPT ensemble for 1 ns at the corresponding pressure and temperature, $T = (T_{COLD} + T_{HOT})/2$. The width of the thermostatting regions was set to $\simeq 0.1$ nm. The NEMD simulations were performed by switching on the thermostats at the temperatures T_{COLD} and T_{HOT}, at constant volume. These simulations were run for several ns, to ensure the stationary state was reached. We then performed production runs and accumulate statistics over 16 ns. The trajectories were analysed every 100 time steps to construct the temperature, density and concentration profiles, by dividing the simulation box into 100 sampling volumes along the direction of the thermal gradient, z. The temperature profile was calculated using the equipartition principle by sampling the velocities of the water molecules and the ions.

The Soret coefficient was obtained from the analysis of the molar fraction, ∇x_1, and temperature, ∇T, gradients:[1]

$$s_T = -\frac{1}{x_1 x_2}\left(\frac{\nabla x_1}{\nabla T}\right)_{J_1=0} \approx -\frac{1}{x_1}\left(\frac{dx_1}{dT}\right)_{J_1=0}, \qquad (2)$$

where x_1 and x_2 represent the molar fraction of the salt and the solvent, respectively, and the J_1 the mass flux of salt. Since the amount of solvent exceeds considerably the amount of salt employed, we used the approximation shown on the right-hand side of eqn (2). Iacopini *et al.*[16] have shown that the empirical equation, $s_T(T) = s_T^\infty[1 - \exp((T_0 - T)/\tau)]$, describes well the temperature dependence of the Soret coefficient of colloidal suspensions. We have also found that this equation accurately represents the temperature dependence of the Soret coefficient of alkali halide solutions[12]. s_T^∞ and T_0 in the equation above represent the asymptotic limit of the Soret coefficient and the inversion temperature, respectively, and τ determines the temperature dependence of s_T. Using eqn (2) along with the Iacopini et al.[16] equation we derived the following relationship,

$$b(T) = b_0 \exp[-s_T^\infty(T + \tau e^{\frac{T_0 - T}{\tau}} + k)] \qquad (3)$$

where $b(T)$ is the molality at temperature T, b_0 is the average molality of the solution and s_T^∞, and T_0, τ and k are fitting parameters. eqn (3) provides an excellent fitting of all our NEMD data.

The standard deviation of the concentration profiles and the Soret coefficients were obtained from the analysis of 20 or 15 independent trajectories (16 ns each) for RES and UNRES simulations, respectively. The analyses involving changes in the Lennard-Jones parameters and the ion masses were performed using 15 or 10 independent trajectories, respectively.

Results and Discussion

Fig. 1 shows a typical snapshot of the simulation cell employed in this work and representative results for the temperature and salt molality profiles in the stationary state. One noticeable feature in the molality profiles are the maxima, which define the inversion temperature, and that vary with salt concentration (see Fig. 1). At the maxima the Soret coefficient is equal to zero. We observe maxima in the temperature range investigated at concentrations ≤ 3.7 mol kg^{-1}. These maxima were used to represent the inversion points in the inset of Fig. 2. For higher concentrations, the inversion temperatures were estimated from the fitting to eqn (3).

The Soret coefficients were computed from the analysis of the temperature and molar fraction profile using eqn (2), as described in Section 2. Numerical results are reported in the ESI. Fig. 2 reports the dependence of the computed Soret coefficients on the concentration and temperature. This dependence can be fitted accurately to the Iacopini *et al.* empirical equation.[16] The simulated coefficients are of the order, $\sim 10^{-3}$ K^{-1}, in agreement with previous experimental and simulation studies of alkali halide solutions.[10–12,25]

Our results show convincingly the existence of an inversion temperature, T_0, in the Soret coefficient of LiCl. Below 300 K, and for a wide range of salt concentrations, the solutions studied in this work are thermophilic, $s_T < 0$. We find that the inversion

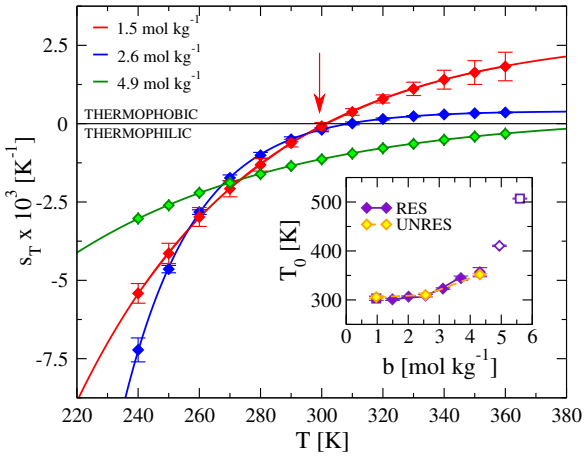

Fig. 2 Temperature dependence of the Soret coefficient for several LiCl salt concentration at 600 bar. The red arrow indicates the temperature at which $s_T = 0$ for 1.5 mol kg^{-1}.(inset) Dependence of the inversion temperature on the salt concentration, calculated using the RES-NEMD and UNRES-NEMD methods. The squares for 1.0 mol kg^{-1} and 5.6 mol kg^{-1} are data from ref. 25. The empty symbols at high concentrations represent the predicted T_0 values obtained from the fitting. See text for details.

temperature of the Soret coefficient increases significantly with salt concentration (see inset of Fig. 2), particularly in the 3.5 – 5.6 mol kg^{-1} concentration regime. The results indicate that high salt concentrations favour thermophilic solutions at ambient temperature. This conclusion is consistent with experimental observations, which reported an overall thermophilic response in LiCl solutions at salt concentrations similar to those studied here.[11] However, the temperature dependence of the thermophilic response was not investigated in the experiments.

To test the reproducibility of our results we performed additional simulations with a different implementation of the NEMD method, namely, the UNRES approach (see Section 2 for further details). The results obtained with this method are in excellent agreement with those obtained with the RES one (see inset Fig. 2). This agreement supports the robustness and accuracy of our data.

NEMD simulations at low temperatures, $\sim$ 240 K, where the solutions are thermophilic, provide theoretical support for the existence of minima in the Soret coefficient.[25] We have expanded the analysis of the temperature dependence of such minima (see Fig. 3). Our simulations reveal a continuum variation in the slope of the Soret coefficient with salt concentration. At high temperatures ($T > 310$ K) the strength of the thermophoretic response decreases with increasing salt concentration, while at lower temperatures it becomes independent on concentration ($270 < T < 310$ K). At lower temperatures the observation of the minima is evident. The simulations indicate that the strength of the minimum decreases with increasing temperature, and it disappears above $\sim$ 260 K. Although these temperatures are below the freezing temperature of pure water, we note that the melting temperature of SPC/E water at 1 bar pressure is lower than the experimental one, $\sim$ 215 K.[41] Also, it is known that addition of salt results in a reduction of the melting temperature of real water. For example, LiCl aqueous solutions of $\sim$ 1.3 mol kg^{-1} or $\sim$ 4.4 mol kg^{-1} induce a freezing point depression of 5.11 K or 25.44 K, respectively.[42] The minimum in our model appears at high concentrations $\sim$ 2.5 mol kg^{-1}, *vs* 0.56 mol kg^{-1} estimated in experiments. This shift could be connected either to the force field employed here or possibly to the different pressure conditions since the experiments were performed at standard pressure. This point can be addressed by examining the pressure dependence of the Soret coefficient (see data in Fig. 3 and ref. 25). We find that at much lower pressures 100 bar, the minimum in the Soret coefficient is still present. Overall, the Soret coefficient is fairly insensitive to pressures changes in the range, 100 – 600 bar. The pressure dependence of the Soret coefficient has not been studied systematically in experiments of alkali halide solutions, although such dependence should be of interest to understand thermodiffusion under non-standard conditions, *e.g.* in geothermally heated water. High-pressure measurements have been performed before to study thermodiffusion of a binary mixture in porous media. Some of these studies show a slight decrease of the Soret coefficients with increasing pressure.[43–49] Our simulations indicate that the Soret coefficient would not undergo significant changes in the pressure and temperature ranges studied here. Our results, therefore, indicate that the differences between simulation and experiments are likely connected to the force-field.

It is remarkable that the model employed here reproduces the complex behaviour of the Soret coefficient of LiCl solutions. Fig. 3-right summarises the complex response of LiCl solution to thermal gradients as a function of temperature and salt concentration. This plot highlights the importance of the thermophilic region as a regime where the minima in the Soret coefficient are observed, and also where this coefficient features rapid variations below 280 K and between 1 – 3 mol kg^{-1} concentrations. At the minimum, the Soret coefficient is significant, $s_T = -7.22 \pm 0.38 \times 10^{-3}$ K^{-1}, and much larger than the coefficients often measured at standard conditions, which are of the order of $\sim 2-3 \times 10^{-3}$ K^{-1}. Our simulations indicate that high salt concentrations and low temperatures favour the thermophilic states, while high temperatures and low salt concentrations favour thermophobic states (see Fig. 3-left and Fig. 3-right). These predictions await experimental verification.

We have shown that our model predicts the main physical behaviour of thermodiffusion in aqueous solutions. In the following, we use our model to gain microscopic insight into the dependence of the minimum of the Soret coefficient with the ion-water interactions. We expect that the polarization of the water molecules around the ions will influence the thermodiffusive response of the LiCl salt and that this response will depend on the ion size since smaller ions generate stronger electrostatic fields. To address this question we performed additional computations varying the Lennard-Jones effective diameter of the lithium cation. The diameter was increased/decreased by 0.05 nm $\sigma_{Li^+,+0.05} = 0.2006$ nm, and $\sigma_{Li^+,-0.05} = 0.1006$ nm.

Fig. 4 - middle panel shows the radial distribution function for the cations of different sizes at a concentration of 2.5 mol kg^{-1}, which is close to the concentration at which we observe

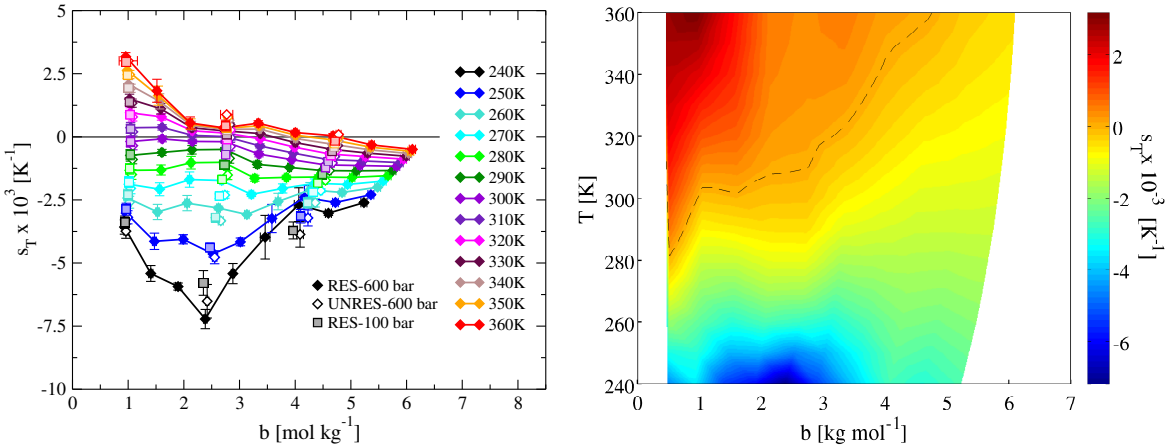

Fig. 3 LiCl Soret coefficient dependence on molality for several isotherms. (left) The full diamonds and full squares represent the NEMD simulations performed with the RES-NEMD method at 600 and 100 bar, respectively. The empty diamonds represent data obtained with the UNRES-NEMD approach using a pressure of 600 bar. The Soret coefficients at 240 K, 270 K and 290 K are taken from ref. 25. (right) Contour diagram showing the dependence of the Soret coefficient on the molality and temperature plane. The color map shows the variation of the Soret coefficient with the thermodynamic conditions. The results were obtained using the RES-NEMD approach and 600 bar. The dashed line indicates the location of the inversion temperature.

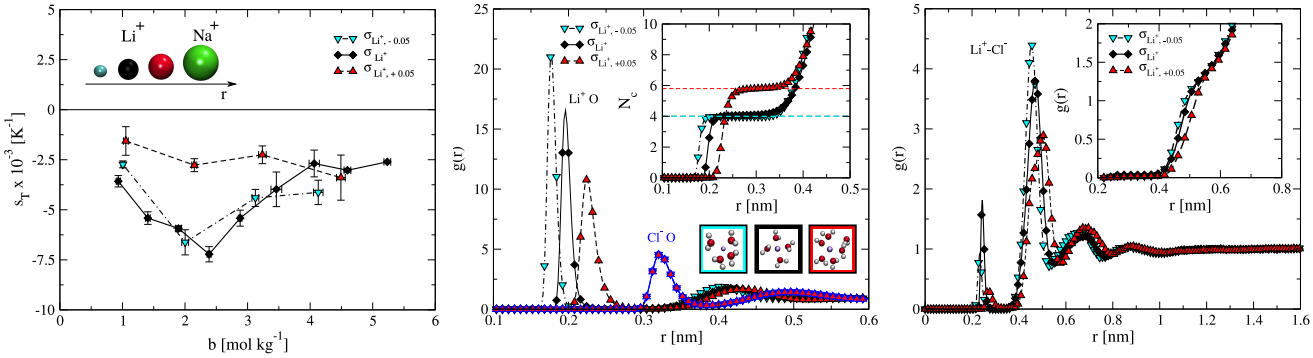

Fig. 4 Thermophoretic and structural changes as a function of the cation size. (Left) Dependence of the Soret coefficient of alkali halide solutions with the Li^+ effective diameter (see main text for details) along the 240 K isotherm. The data labelled σ_{Li^+} correspond to the original Dang's force field (taken from ref. 25). The snapshot illustrates the relative size of the different cations considered. (Middle) Pair correlation functions for the Li-O (black lines with cyan, red and black symbols) and Cl-O (blue lines with cyan, red and black symbols) pairs at T = 240 K and 2.5 mol kg^{-1}, *i.e.* the conditions corresponding to the minimum in s_T in the original Dang model. The inset shows the Li-O running coordination numbers. The snapshots show representative solvation shells for the different cation diameters. (Right) Pair correlation function for the Li-Cl pairs at T = 240 K and 2.5 mol kg^{-1}, and the corresponding running coordination numbers (inset). All the results correspond to 600 bar.

the minimum in the Soret coefficient. The larger diameter, $\sigma_{Li^+,+0.05} = 0.2006$ nm, is between that of Li^+ and Na^+ in the force field by Dang (see snapshots in Fig. 4 - left panel). Larger diameter lead to a reduction of the electrostatic field around the cation and a diminishing polarization of the surrounding water molecules. These effects are reflected in a higher coordination number, 5.8 (see Fig. 4 - middle panel), which is closer to that of Na^+. The solvation structure changes significantly, from a tight tetrahedral solvation shell to a more open structure (see snapshot in Fig. 4-middle panel). On the other hand the smaller cation, $\sigma_{Li^+,-0.05} = 0.1006$ nm, which has a stronger polarizing influence does not modify the coordination number of the original force field nor the main solvation structure (*c.f.* snapshots in Fig. 4 - middle panel), although it introduces noticeable changes in the position of the main peak of the pair correlation function.

At the concentration studied here, 2.5 mol kg^{-1}, the average distance between the cations and anions, assuming they are uncorrelated, is of the order of ~ 0.7 nm. The coulombic interactions bring this distance to a shorter value, 0.4 – 0.5 nm (see Fig. 4 - right) with some (small) degree of ion-pairing. Despite the short cation-ion distance, we find that the solvation shell of the Cl^- is not affected by the modification of the cation diameter (see Fig. 4 - middle panel). Interestingly, for the smallest cation $\sigma_{Li^+,-0.05}$, the Soret coefficient features the same behaviour observed in the original model by Dang for Li^+, namely, we observe a minimum. However, for the bigger cation, which involves a disruption of the tetrahedral water solvation shell, we do not observe a minimum in the Soret coefficient. Instead, we find a smooth decrease of

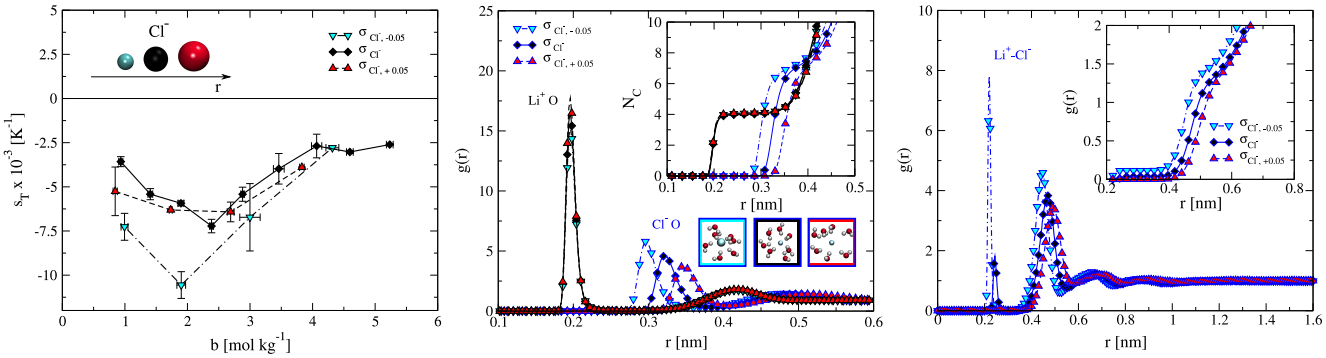

Fig. 5 Thermophoretic and structural changes as a function of the anion size. (Left) Dependence of the Soret coefficient of alkali halide solutions with the Cl^- effective diameter (see main text for details) along the 240 K isotherm. The data labelled σ_{Cl^-} correspond to original Dang's force field (taken from ref. 25). (Middle) Running coordination number (inset) and pair correlation functions for the Li-O (black lines with cyan, red and black symbols) and Cl-O (blue lines with cyan, red and black symbols) pairs at T = 240 K and 2.5 mol kg^{-1}, *i.e.* the conditions corresponding to the minimum in s_T in the original Dang model. The snapshots show the first coordination shell around the Cl^- ion for the three diameters considered in this work. (Right) Pair correlation function for the Li-Cl pairs at T = 240 K and 2.5 mol kg^{-1}, and the corresponding running coordination numbers (inset). All the results correspond to 600 bar.

the coefficient with salt concentration, which resembles the behaviour we observe for LiCl at higher temperatures. At the same time, the increase in the cation size results in a solution that is less thermophilic, as can be inferred by the decrease in the absolute value of the Soret coefficient (see Fig. 4 - left). Our results highlight the strong sensitivity of the Soret coefficient to changes in ion-water interactions and point towards a correlation between the minimum we observe in s_T and the tetrahedral coordination of the Li^+ cation.

To test further this hypothesis we extended our analysis and considered similar size changes in the anion (see Fig. 5). Specifically, we modified the Lennard-Jones effective diameter by $\pm$ 0.05 nm, *i.e.* $\sigma_{Cl^-,+0.05}$ and $\sigma_{Cl^-,-0.05}$. The local structure of the counter ion, Li^+, does not change upon increasing/decreasing the anion size, *i.e.* the Li^+-water correlations are not significantly influenced by changes in the anion diameter. The Cl^--water correlations are significantly modified, though (see coordination numbers and snapshots in Fig. 5 - middle panel). The Cl-O coordination number increases with σ_{Cl^-}: 7.05, 7.15 and 7.34 for $\sigma_{Cl^-,-0.05}$, σ_{Cl^-} and $\sigma_{Cl^-,+0.05}$, respectively. For similar changes in the ion diameter, the Soret coefficient features a smaller dependence with anion size than with cation size. In fact, the minimum in the Soret coefficient is still present for $\sigma_{Cl^-,-0.05}$, and it appears at the same concentration as in the original model. The Li-O coordination number is 4 irrespective of the σ_{Cl^-} value. Again, the appearance of the minimum is consistent with the existence of a tight tetrahedral solvation shell around the Li^+ cation. Our model predicts that smaller anions result in an increase in the magnitude of the Soret coefficient, and the solution becomes more thermophilic as compared with the original LiCl solution.

It is unlikely that the thermophilic character of the lithium salts can be interpreted considering the motion of the isolated ions in the thermal field, rather the solvent contributions need to be accounted for. This notion applies particularly to Li^+, since it is strongly solvated by four water molecules (see Fig. 4 - middle panel). Hence, a description of the thermodiffusive response would need to consider the concerted motion of Li^+ with its corresponding solvation shell.

The minimum in the Soret coefficient appears at intermediate concentrations where non-ideal contributions are expected to become relevant. Indeed the thermodynamic factor of this solution is $\Gamma \sim 1.3$[25] at the concentration and temperature corresponding to the minimum. We show in the right panels of Fig. 4 and Fig. 5, the Li-Cl pair correlation functions, which provide information on the inter-ionic correlations, and possible ion clustering effects. The ionic correlations are less affected by the ion changes than the water-ion ones, although we observe a small increase in the Li-Cl dimerization as the anion diameter decreases. To quantify the number of dimers in the solution we consider that a cation and an anion are "bonded" if the distance between them is smaller than 0.3 nm. This distance corresponds to the region between the first and second peaks in the LiCl pair correlation function, where the correlation function is close to zero (see right panel in Fig. 4 and Fig. 5). The fraction of dimers is small, $\sim$ 13.5% of the total ion pairs, for the system where we observe the highest dimer formation, $\sigma_{Cl^-,-0.05}$. This small fraction indicates that clustering does not play a dominant role in determining the minimum of the Soret coefficients observed here.

It has been shown that the thermal diffusion phenomena can be influenced by physical (atomic mass and size, and moment of inertia of molecules)[50] and chemical factors (solvent-particle and particle-particle interactions).[51] We have analysed the impact of the chemical factors in our previous discussion. To address the impact of physical factors, we modified the anion and cation masses. This investigation is of particular interest. As we consider a classical model, any changes in the ion mass do not influence the structure of the ion-water solvation shell, nor the corresponding hydration free energy. We find that the change in mass does not alter significantly the location and intensity of the minimum (see Fig. 6). The lack of a strong dependence on mass indicates that the minimum in s_T is determined primarily by the hydration structure around the ions and the strong dependence of this structure with ion size.

To complete our structural analysis we computed the number

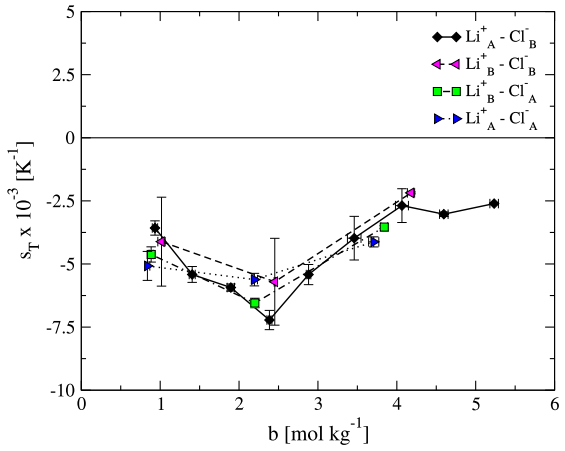

Fig. 6 Soret coefficient of LiCl solutions as a function of molality at 240 K. The NEMD simulations were performed at 600 bar. The subscript "A" refers to the Lithium mass, $m_{Li^+} = 6.941$ g mol^{-1} while the subscript B refers to the Chloride mass, $m_{Cl^-} = 35.453$ g mol^{-1}. The black symbols and full black line correspond to the original Dang's force field and are taken from ref. 25.

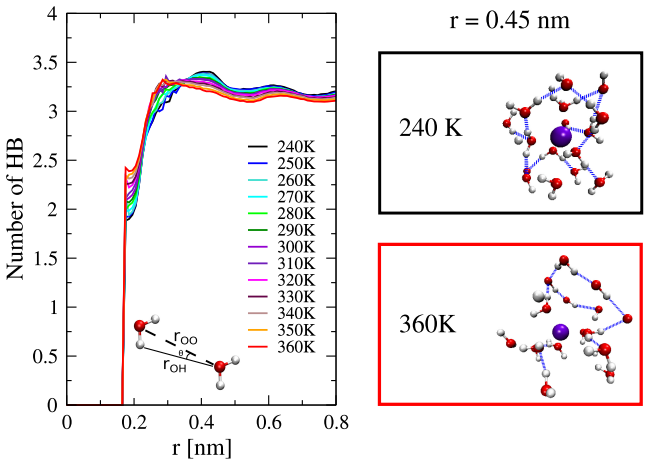

Fig. 7 (Left) Number of hydrogen bonds between water molecules, as a function of the radial distance to the Li^+ cation. The results correspond to 2.5 mol kg^{-1} of LiCl, which is the concentration at which we observe the minimum. (Right) Visualization of the hydrogen bonds (blue lines) in a sphere of radius 0.45 nm around Li^+ at 240 K and 360 K. All the results correspond to the original force field by Dang *et al.*

of hydrogen bonds of the water molecules around the Li^+ cation. Two water molecules were assumed to be hydrogen bonded if the oxygen-oxygen distance (r_{OO} in Fig. 7) is shorter than 0.35 nm and if the angle between the vector connecting the oxygen atoms of the two molecules and the vector connecting the oxygen and the hydrogen in the same molecule (θ in Fig. 7), is smaller than 30°. Fig. 7 shows the dependence of the number of hydrogen bonds with temperature (at the concentration corresponding to the minimum). The number of hydrogen bonds between water molecules in the first solvation shell of Li^+, $r \sim 0.2$ nm is depleted considerably, with the molecules losing about 1 hydrogen bond with respect to the bulk value, ~ 3.6. The hydrogen bond radial profile (Fig. 7) features isosbestic points between 0.2 and 0.4 nm. These values correspond to intermediate distances between the first and second solvation shells of the Li^+ ion. At short distances from Li^+ ($r < 0.3$ m) the number of hydrogen bonds increases with temperature, while it decreases at longer distances ($r > 0.4$ nm). On the right panel of Fig. 7, we represent snapshots of the water molecules around the anion Li^+ in a sphere of radius 0.45 nm, that illustrate the formation of the hydrogen bonds between the water molecules. These results indicate a significant reorganization of the hydrogen bond structure, with a stronger ordering at lower temperatures. At the temperature corresponding to the minimum in s_T, the coordination shell features a stronger structure, and this is reflected in the reduction in the average number of hydrogen bonds per water molecule (*c.f.* snapshots in Fig. 7 and see Fig. 7 - left). The enhanced structuring at low temperatures is consistent with the oscillatory behaviour observed in the number of hydrogen bonds as a function of the water-Li^+ radial distance.

Summary and Conclusions

We have investigated using Non-Equilibrium Molecular Dynamics simulations the Soret coefficient of lithium chloride solutions at medium-high concentrations 1 – 5.6 mol kg^{-1}. We find a complex thermodiffusive behaviour, characterized by the existence of a temperature inversion in the Soret coefficient, with the solution turning from thermophilic at low temperatures to thermophobic at high temperatures. We show that at high saline concentrations, LiCl solutions are mostly thermophilic in a wide range of temperatures up to 400 – 500 K, *i.e.* the salt will preferentially drift towards the hot region. The dependence predicted in this work awaits experimental verification, and it might be of interest to advance our understanding of thermodiffusion processes in extreme conditions, such as those present in hydrothermal vents.

The minimum of the Soret coefficient of LiCl is found to depend significantly on the temperature too. At high temperatures, the minimum disappears or it is shifted to concentrations outside the range investigated here. The ion-solvent interactions have a considerable impact on the observation of the minima. Salts consisting of small cations, which stabilise a tight tetrahedral hydration shell, show the minimum. This minimum disappears for large cations, for which the tetrahedral hydration shell is considerably disrupted. Our work highlights the importance of the Li^+-solvent interaction in determining the minimum in the Soret coefficient. Understanding the exact location of the minimum with salt concentation will require further investigations, in order to establish correlations between the location of the minimum and the solution composition. The minimum reported here appears in a concentration region where non-ideal effects are relevant, and where the Debye length is of the order of the ion diameter (~ 0.2 nm), and hence, the electrostatic interactions are screened significantly. We, therefore, expect that these non-ideal effects are responsible for the observation of minimum in the Soret coefficient.

We investigated the relevance of ion mass on the thermodiffusion and the Soret coefficient by modifying the mass of cations and anions independently. We find that the mass plays a minor

role in defining the Soret coefficient of these solutions, hence supporting the key role of ion-water interactions in determining the thermodiffusive behaviour of the solution.

Our results highlight the important role of the Li^+ solvation structure in defining the thermodiffusion response of the LiCl solution. Theoretical interpretations of the thermodiffusion of this ion should take into account that it forms fairly stable $[Li[(H_2O)_4]^+$ clusters, which will likely move as a single unit in the thermal field. Further simulation studies for other salts will help to establish a microscopic connection between the ion solvation properties and the Soret coefficient. Such information is important to rationalize the thermophoretic response of solutes in aqueous solutions, and more generally to develop predictive theories to describe and predict the Soret and Seebeck effects in aqueous media.

Acknowledgements

We thank the EPSRC (EP/J003859/1) and NFR (Project No. 221675) for financial support. We acknowledge the Imperial College High-Performance Computing Service for providing computational resources. We also thank Prof. Jean Colombani for many useful discussions and for providing ref. 13.

References

1 S. de Groot and P. Mazur, *Non-equilibrium Thermodynamics*, Dover Publications, 1984.

2 F. Bresme, A. Lervik, D. Bedeaux and S. Kjelstrup, *Phys. Rev. Lett.*, 2008, **101**, 020602.

3 F. Römer, F. Bresme, J. Muscatello, D. Bedeaux and J. Rubi, *Phys. Rev. Lett.*, 2012, **108**, 105901.

4 C. D. Daub, J. Tafjord, S. Kjelstrup, D. Bedeaux and F. Bresme, *Phys. Chem. Chem. Phys.*, 2016, **18**, 12213–12220.

5 I. Iriarte-Carretero, M. A. Gonzalez, J. Armstrong, F. Fernandez-Alonso and F. Bresme, *Phys. Chem. Chem. Phys.*, 2016, **18**, 19894–19901.

6 C. Ludwig, *Diffusion zwischen ungleich erwärmten Orten gleich zusammengesetzter Lösungen*, Sitz. Ber. Akad. Wiss. Wien Math-Naturw. Kl., 1856, p. 539.

7 C. Soret, *Archives des sciences physiques et naturelles, Bibliothèque Universelle*, 1879, **2**, 48–61.

8 C. Mast and B. D., *Phys. Rev. Lett.*, 2010, **104**, 188102.

9 C. Wienken, P. Baaske, U. Rothbauer, D. Braun and S. Duhr, *Nat. Commun.*, 2010, **1**, 100.

10 F. S. Gaeta, G. Perna, G. Scala and F. Bellucci, *J. Phys. Chem.*, 1982, **86**, 2967–2974.

11 J. Colombani, J. Bert and J. Dupuy-Philon, *J. Chem. Phys.*, 1999, **110**, 8622–8627.

12 F. Römer, Z. Wang, S. Wiegand and F. Bresme, *J. Phys. Chem. B*, 2013, **117**, 8209–8222.

13 C. Wood and W. Haksworth, *J. South African Chem. Inst.*, 1971, **24**, 170–176.

14 S. Wiegand, *J. Phys.: Condens. Matter*, 2004, **16**, R357.

15 G. Wittko and W. Köhler, *EPL (Europhysics Letters)*, 2007, **78**, 46007.

16 S. Iacopini, R. Rusconi and R. Piazza, *Eur. Phys. J. E*, 2006, **19**, 59–67.

17 S. Kjelstrup and D. Bedeaux, *Non-Equilibrium Thermodynamics of Heterogeneous Systems*, World Scientific, 1st edn., 2008.

18 D. Reguera, J. M. Rubi and J. M. G. Vilar, *J. Phys. Chem. B*, 2005, **109**, 21502–21515.

19 K. Alexander, *Phys. Chem. (Leipzig)*, 1954, **203**, 213–227.

20 W. Köhler and B. Müller, *J. Chem. Phys.*, 1995, **103**, 4367–4370.

21 S. Duhr and D. Braun, *Proc. Natl. Acad. Sci.*, 2006, **103**, 19678–19682.

22 R. Kita, S. Wiegand and J. Luettmer-Strathmann, *J. Chem. Phys.*, 2004, **121**, 3874–3885.

23 H. Brenner, *Phys. Rev. E*, 2010, **82**, 036325.

24 S. Putnam, D. Cahill and G. Wong, *Langmuir*, 2007, **23**, 9221–9228.

25 S. Di Lecce, T. Albrecht and F. Bresme, *Scientific Reports*, 2017, **7**, 1–10.

26 P. E. Mason, S. Ansell, G. W. Neilson and S. B. Rempe, *J. Phys. Chem. B*, 2015, **119**, 2003–2009.

27 F. Römer, A. Lervik and F. Bresme, *J. Chem. Phys.*, 2012, **137**, 074503.

28 G. Bussi, D. Donadio and M. Parrinello, *J. Chem. Phys.*, 2007, **126**, 014101.

29 B. Hess, C. Kutzner, D. van der Spoel and E. Lindahl, *J. Chem. Theory Comput.*, 2008, **4**, 435–447.

30 J. Armstrong and F. Bresme, *J. Chem. Phys.*, 2013, **139**, 014504.

31 S. Plimpton, *J. Comput. Phys.*, 1995, **117**, 1–19.

32 H. J. C. Berendsen, J. R. Grigera and T. P. Straatsma, *J. Phys. Chem.*, 1987, **91**, 6269–6271.

33 L. X. Dang, *J. Chem. Phys.*, 1992, **96**, 6970–6977.

34 L. X. Dang and B. C. Garrett, *J. Chem. Phys.*, 1993, **99**, 2972–2977.

35 D. E. Smith and L. X. Dang, *J. Chem. Phys.*, 1994, **100**, 3757–3766.

36 L. X. Dang, *J. Am. Chem. Soc.*, 1995, **117**, 6954–6960.

37 A. Wynveen and F. Bresme, *J. Chem. Phys.*, 2010, **133**, 144706.

38 C. D. Daub, P.-O. Åstrand and F. Bresme, *J. Phys. Chem. A*, 2015, **119**, 4983–4992.

39 T. Darden, D. York and L. Pedersen, *J. Chem. Phys.*, 1993, **98**, 10089–10092.

40 R. E. Isele-Holder, W. Mitchell and A. E. Ismail, *J. Chem. Phys.*, 2012, **137**, 174107.

41 C. Vega, E. Sanz and J. L. F. Abascal, *J. Chem. Phys.*, 2005, **122**, 114507.

42 W. H. Rodebush, *J. Am. Chem. Soc.*, 1918, **40**, 1204–1213.

43 C. Giraudet, F. Croccolo, G. Galliero, G. Pijaudier-Cabot, S. V. Vaerenbergh, M. Z. Saghir, F. Montel and H. Bataller, *Comptes Rendus Mécanique*, 2013, **341**, 340 – 347.

44 C. Giraudet, H. Bataller and F. Croccolo, *The European Physical Journal E*, 2014, **37**, 107.

45 C. Jiang, T. Jaber, H. Bataller and M. Saghir, *International Journal of Thermal Sciences*, 2008, **47**, 126 – 135.

46 S. Srinivasan and M. Z. Saghir, *The Journal of Chemical Physics*, 2009, **131**, 124508.

47 P. Urteaga, M. M. Bou-Ali, D. A. de Mezquia, J. Santamaría, C. Santamaría, J. A. Madariaga and H. Bataller, *Review of Scientific Instruments*, 2012, **83**, 074903.

48 S. VanVaerenbergh, S. Srinivasan and M. Z. Saghir, *The Journal of Chemical Physics*, 2009, **131**, 114505.

49 S. V. Vaerenbergh, S. Srinivasan and M. Z. Saghir, *The Journal of Chemical Physics*, 2010, **132**, 099901.

50 C. Debuschewitz and W. Köhler, *Phys. Rev. Lett.*, 2001, **87**, 055901.

51 S. Wiegand, N. Hui and K. Rio, *J. Non-Equilib. Thermodyn.*, 2007, **32**, 193–201.